

Neutral pion photoproduction on the nucleon near threshold

S. Nozawa

TRIUMF, 4004 Wesbrook Mall, Vancouver, British Columbia, Canada V6T 2A3

T.-S. H. Lee*

*Argonne National Laboratory, Argonne, Illinois 60439
and TRIUMF, 4004 Wesbrook Mall, Vancouver, British Columbia, Canada V6T 2A3*

B. Blankleider

*Paul Scherrer Institute, CH-5232 Villigen PSI, Switzerland
(Received 4 August 1989)*

Neutral pion photoproduction on the nucleon near threshold is investigated using a dynamical model. Analytic properties of the final-state interaction amplitude in the energy region near π^+n production threshold are examined in detail. It is shown that the commonly used procedure, based on an analytical continuation of the K matrix to the unphysical region, is not compatible to an approach incorporating full off-energy-shell dynamics. Our calculation indicates that the final-state interaction amplitude derived from a dynamical model could involve large cancellation between the different pion photoproduction mechanisms. This leads to the surprising result that the final-state interaction effect due to the intermediate π^0p state can be as important as that due to the π^+n intermediate state. At threshold, we obtain $E_{0+} = -1.92 \times 10^{-3}/m_{\pi^+}$. This number is close to the measured value of $E_{0+} = -1.5 \times 10^{-3}/m_{\pi^+}$. No violation of the low-energy theorem is required to obtain good agreement between the calculated total cross sections and experimental data from threshold to about 400-MeV incident photon energy.

I. INTRODUCTION

It has been reported for some time that the E_{0+} amplitude extracted from analyses^{1,2} of threshold neutral pion photoproduction data seems incompatible with the well-established low-energy theorem.³ This is very surprising since no violation of the low-energy theorem has been observed for charged pion production. In this paper we explore this problem within a dynamical model⁴⁻⁶ in which the pion-nucleon interaction is described with πNN and $\pi N\Delta$ vertices, and a background potential; the pion photoproduction mechanisms are deduced from low-order Feynman amplitudes calculated from an effective Lagrangian. A similar approach has been recently taken by Yang⁷ to demonstrate the role of off-energy-shell πN final-state interaction (FSI) in interpreting the data. We will present a much more detailed formulation of the FSI dynamics, which is needed for a clear understanding of several new findings emerging from our calculations.

Let us first recall what has been done in arriving at the contradiction to the low-energy theorem. A nontrivial problem arises from the fact that the threshold of the $\gamma p \rightarrow \pi^0 p$ reaction is 144.7 MeV (all photon energies are specified in the laboratory frame) which is 6.7 MeV lower than the threshold of π^+ production which can contribute to π^0 production through the charge-exchange process $\gamma p \rightarrow \pi^+ n \rightarrow \pi^0 p$. To evaluate this contribution, one needs to define the *off-shell* πN charge-exchange scattering amplitude. Evidently, this cannot be obtained from the experimental data of πN scattering without making

theoretical assumptions. In the analyses of Refs. 1 and 2, it is assumed that, in the energy region near the π^0 production threshold, the s -wave multipole amplitude can be written as

$$E_{0+} = \hat{E}_{0+}(\gamma p \rightarrow \pi^0 p) + (\text{FSI}). \quad (1.1a)$$

Here $\hat{E}_{0+}(\gamma p \rightarrow \pi^0 p)$ is extracted from the E_{0+} data by assuming that the final-state interaction can be described with a K -matrix approach⁸ which gives

$$(\text{FSI}) = ik_t a_{\pi^+ n \rightarrow \pi^0 p} E_{0+}(\gamma p \rightarrow \pi^+ n). \quad (1.1b)$$

In Eq. (1.1b), the π^+n relative momentum k_t is evaluated from the on-energy-shell condition $E = E_n(k_t) + E_{\pi^+}(k_t)$, where $E_n(k) = (m_n^2 + k^2)^{1/2}$ and $E_{\pi^+}(k) = (m_{\pi^+}^2 + k^2)^{1/2}$. With the mass parameters $m_{\pi^0} = 134.9630$ MeV, $m_{\pi^+} = 139.5673$ MeV, $m_p = 938.2796$ MeV, and $m_n = 939.5731$ MeV, we have, at the π^0 production threshold ($E = m_{\pi^0} + m_p$), $k_t = i 0.19 \text{ fm}^{-1}$. The charge-exchange scattering length, $a_{\pi^+ n \rightarrow \pi^0 p}$, is calculated from the πN S_{11} and S_{31} scattering lengths⁹ $a^{1/2} = (0.173 \pm 0.003)/m_{\pi^+} \simeq 0.245 \text{ fm}$ and $a^{3/2} = (-0.101 \pm 0.004)/m_{\pi^+} \simeq -0.143 \text{ fm}$ by multiplication with appropriate isospin Clebsch-Gordan coefficients. By using these empirical numbers and the value $E_{0+}(\gamma p \rightarrow \pi^+ n) = 28.3 \pm 0.5$ (all multipoles are in the standard unit $10^{-3}/m_{\pi^+}$), we find that $(\text{FSI}) \simeq -1.0$. It is the use of this (FSI) value that led to the result^{1,2} $\hat{E}_{0+}(\gamma p \rightarrow \pi^0 p) = -0.5 \pm 0.3$ in conflict with the low-

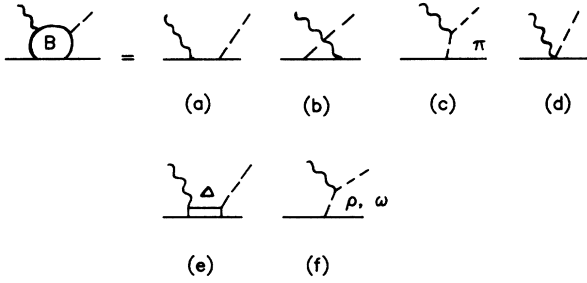


FIG. 1. The pion photoproduction mechanisms considered in this work.

energy theorem value of -2.4 . Inserting the reported value $\hat{E}_{0+}(\gamma p \rightarrow \pi^0 p) = -0.5 \pm 0.3$ into Eq. (1.1), we then have

$$E_{0+} \simeq -0.5 - 1.0 = -1.5. \tag{1.2}$$

We note here that any theoretical model including effects of FSI should compare directly with the experimental value of -1.5 . It is clear from Eq. (1.2) that the significance of the often-mentioned “unexpected value” -0.5 depends strongly on the validity of using the large FSI correction -1.0 , deduced from the K -matrix approach. The FSI has also been investigated by Yang,⁷ Davidson and Mukhopadhyay,¹⁰ and Araki.¹¹ Their values are all different from the value -1.0 .

We further note here that the analyses of Refs. 1 and 2 also made an assumption that for the other two relevant multipoles, M_{1+}/qk and M_{1-}/qk are constant from threshold up to about 180 MeV. This could be reasonable, but needs to be confirmed since the cross section calculation involves interference between different multipoles, and the small amplitudes could play important roles in fitting the differential cross section data.

We now emphasize that Eq. (1.1) results from a particular choice⁸ for the analytical continuation of the K matrix to the unphysical region. On the other hand, the analytic continuation of the K matrix to the unphysical re-

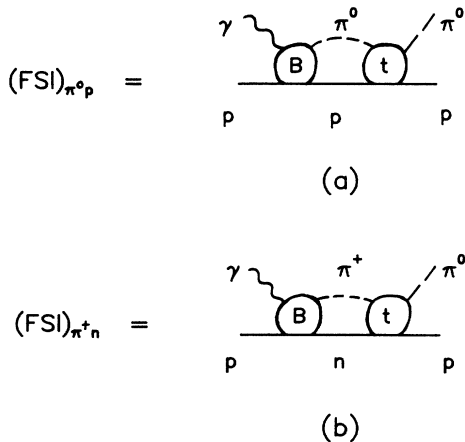


FIG. 2. Graphical representation of the final-state interaction terms (FSI) of Eq. (2.1). B is the photoproduction Born term and t is the $\pi N t$ matrix.

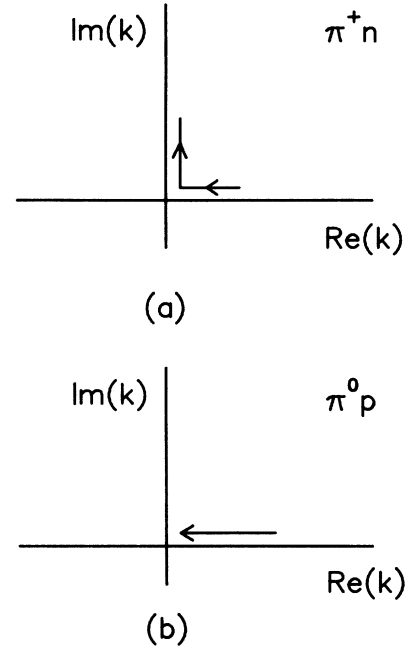


FIG. 3. Trajectories of the πN propagator singularity, shown for the case where the energy moves from above to below the $\pi^+ n$ production threshold.

gion is not unique and depends on the underlying dynamics. This arbitrariness is inherent in any attempt to specify the FSI without solving a “dynamical equation.” In a dynamical approach, as developed in Refs. 4–6, the FSI includes the full off-energy-shell contribution and can be explicitly calculated from the underlying Hamiltonian. The objective of this work is to reveal this dynamical feature, using the model we have recently proposed.⁶ This will allow us to examine whether Eq. (1.1) is compatible with a dynamical model.

In Sec. II, we recall a relevant formula of Ref. 6 to exhibit, within a dynamical approach, the analytical properties of the pion photoproduction amplitudes at energies

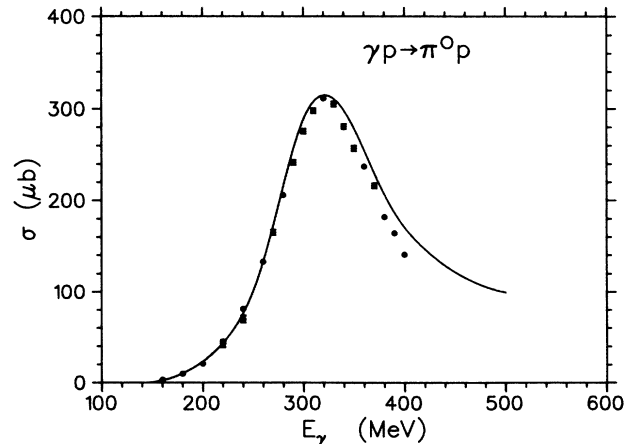


FIG. 4. Calculated total cross section of $\gamma p \rightarrow \pi^0 p$ reaction up to 500-MeV photon laboratory energy. The experimental data are taken from Ref. 15.

near (below and above) π^+ threshold. We will demonstrate how the cusp effect emerges from our formulation, without introducing any *ad hoc* prescription. It will be seen that Eq. (1.1) can be obtained from a dynamical model only when very drastic simplifications are introduced in the calculation of the FSI. In Sec. III, we will demonstrate that the dynamical model of Ref. 6 can give a satisfactory description of the total cross section data for $\gamma p \rightarrow \pi^0 p$. The considered pion photoproduction dynamics remains rigorously constrained by the low-energy theorem. More importantly, we will present a detailed analysis of our FSI calculation, clearly demonstrating the radical difference between a dynamical approach and the approach based on Eq. (1.1). The needed future investigations will also be discussed.

II. ANALYTICAL PROPERTIES OF THE PHOTOPRODUCTION AMPLITUDE

Since our model has been presented in detail in Ref. 6, we will only mention some crucial points of our approach and recall relevant equations. The main feature of a dynamical model is that the πN final-state interaction is necessarily determined not only by the πN scattering phase shifts, as required by the Watson theorem,¹² but also by the half-off-shell scattering t matrix which describes the πN wave function in the interaction region. For the considered $\gamma p \rightarrow \pi^0 p$ reaction, each pion photoproduction multipole amplitude is determined by the following equation⁶ (all partial wave quantum numbers are suppressed):

$$M_{\pi^0 p \leftarrow \gamma p}(k_0, q) = B_{\pi^0 p \leftarrow \gamma p}(k_0, q) + (\text{FSI})_{\pi^0 p} + (\text{FSI})_{\pi^+ n}, \quad (2.1)$$

where k_0 and q are momenta of the pion and photon in the center-of-mass frame, respectively. In Eq. (2.1), B is the Born term calculated from the Feynman amplitudes of Fig. 1. Note that our Born term includes the Δ term,

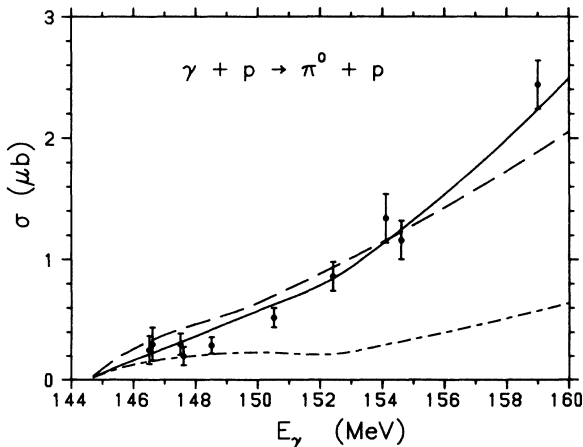


FIG. 5. Calculated total cross section of $\gamma p \rightarrow \pi^0 p$ reaction near threshold. The solid line is the full calculation (B +FSI) and the dashed line is the Born term contribution (B). The dash-dotted line is the contribution from the E_{0+} multipole amplitude only. Experimental data are taken from Ref. 1.

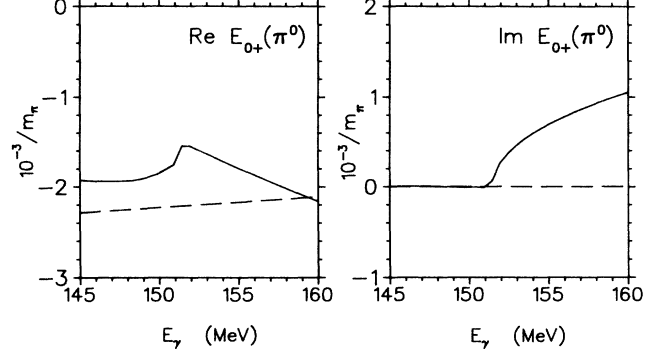


FIG. 6. E_{0+} multipole amplitude of $\gamma p \rightarrow \pi^0 p$ reaction near threshold. The solid line is the full calculation (B +FSI), and the dashed line is the Born term contribution (B).

Fig. 1(e), and the vector meson (ρ and ω) exchange terms, Fig. 1(f). The on-shell momentum k_0 is calculated from $E = E_p(k_0) + E_{\pi^0}(k_0)$. As usual, we assume that no explicit description of the Coulomb interaction is needed, although its effect in contributing to isomultiplet mass splittings is of course included by using empirical masses.

The FSI term involves an integration over the half-off-shell πN t matrix (as illustrated in Fig. 2)

$$(\text{FSI})_{\pi N} = \int_0^\infty dk k^2 \frac{t_{\pi^0 p \leftarrow \pi N}(k_0, k, E) B_{\pi N \leftarrow \gamma p}(k, q)}{E - E_N(k) - E_\pi(k) + i\epsilon}, \quad (2.2)$$

where πN denotes $\pi^0 p$ or $\pi^+ n$. Note that the pole position of the propagator in Eq. (2.2) depends on the masses of the intermediate πN state. In Fig. 3, we show that as the energy becomes smaller than the $\pi^+ n$ threshold, the pole position of the $\pi^+ n$ propagator shifts from the real axis to the imaginary axis. As will be seen later, this is the dynamical origin of the cusp effect.

To extract an overall πN phase from Eq. (2.1), we recall the well-known relation between the t and the K matrix (called the R matrix in Refs. 6 and 13)

$$t(E) = K(E) - i\pi t(E)\delta(E - H_0)K(E), \quad (2.3)$$

where H_0 is the sum of the free-energy operators of the pion and the nucleon. Taking into account the mass differences between the two possible intermediate states $\pi^0 p$ and $\pi^+ n$, we have

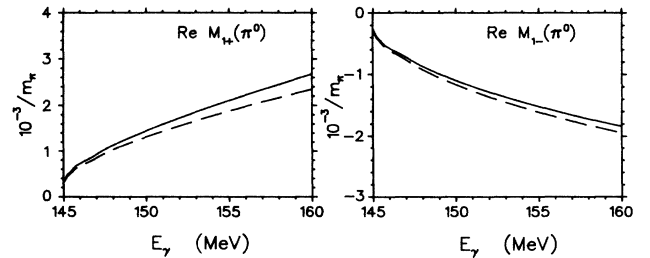


FIG. 7. Real part of the M_{1+} and M_{1-} multipole amplitudes of $\gamma p \rightarrow \pi^0 p$ reaction near threshold. The solid line is the full calculation (B +FSI) and the dashed line is the Born term contribution (B).

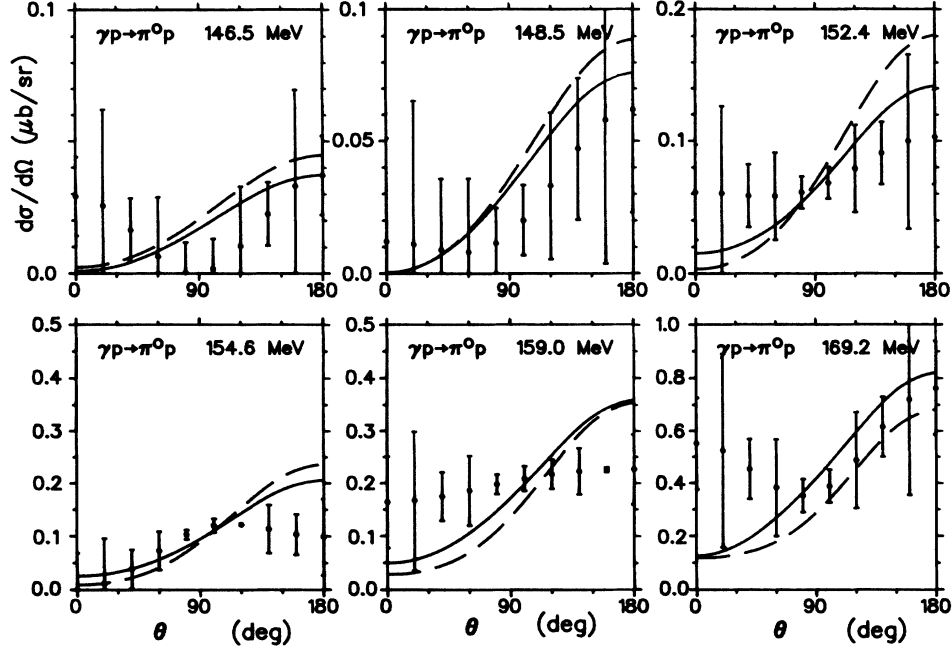


FIG. 8. Calculated differential cross sections of $\gamma p \rightarrow \pi^0 p$ reaction near threshold. The solid line is the full calculation ($B + \text{FSI}$) and the dashed line is the Born term contribution (B). The experimental data are generated from coefficients A , B , C , and their associated errors listed in Table I of Ref. 1.

$$t_{\pi^0 p \leftarrow \pi N}(k_0, k, E) = K_{\pi^0 p \leftarrow \pi N}(k_0, k, E) - i \int_0^\infty dk' t_{\pi^0 p \leftarrow \pi^0 p}(k_0, k', E) \rho_{\pi^0 p}(k') \delta(k' - k_0) K_{\pi^0 p \leftarrow \pi N}(k', k, E) - i \int_0^\infty dk' t_{\pi^0 p \leftarrow \pi^+ n}(k_0, k', E) \rho_{\pi^+ n}(k') \delta(k' - k_t) K_{\pi^+ n \leftarrow \pi N}(k', k, E), \quad (2.4)$$

where $\pi N = \pi^0 p$ or $\pi^+ n$, and $\rho_{\pi N}(k) = \pi k E_N(k) E_\pi(k) / [E_N(k) + E_\pi(k)]$. Note that the last term of Eq. (2.4) involves an integration over a δ function containing a $\pi^+ n$ on-shell momentum k_t , defined by $E = E_n(k_t) + E_{\pi^+}(k_t)$. In the energy region just below the threshold for $\pi^+ n$ ($E < m_n + m_{\pi^+}$), $k_t = i|k_t|$, and hence, the last term in Eq. (2.4) vanishes. Evaluation of Eq. (2.4) for $k = k_t$ and $\pi N = \pi^+ n$ leads to an equation which is then used to cast Eq. (2.4) into the form

$$t_{\pi^0 p \leftarrow \pi N}(k_0, k, E) = [1 - i \rho_{\pi^0 p}(k_0) t_{\pi^0 p \leftarrow \pi^0 p}(k_0, k_0, E)] \hat{K}_{\pi^0 p \leftarrow \pi N}(k_0, k, E), \quad (2.5a)$$

where

$$\hat{K}_{\pi^0 p \leftarrow \pi N}(k_0, k, E) = K_{\pi^0 p \leftarrow \pi N}(k_0, k, E) - i \theta(E - m_n - m_{\pi^+}) F_{\pi^0 p \leftarrow \pi^+ n}(k_0, k_t, E) K_{\pi^+ n \leftarrow \pi N}(k_t, k, E) \quad (2.5b)$$

with

$$F_{\pi^0 p \leftarrow \pi^+ n}(k_0, k_t, E) = \frac{\rho_{\pi^+ n}(k_t) K_{\pi^0 p \leftarrow \pi^+ n}(k_0, k_t, E)}{1 + i \theta(E - m_n - m_{\pi^+}) \rho_{\pi^+ n}(k_t) K_{\pi^+ n \leftarrow \pi^+ n}(k_t, k_t, E)}. \quad (2.5c)$$

TABLE I. Real parts of the multipole amplitudes, calculated from our dynamical model, at the threshold energies E_{th} . B is the contribution from the Born term, and $\text{FSI} = (\text{FSI})_{\pi^0 p} + (\text{FSI})_{\pi^+ n}$ is the final-state interaction contribution.

Reaction (Threshold energy)		$\text{Re}(E_{0+})$ $10^{-3}/m_{\pi^+}$	$\text{Re}(E_{1+})$ $10^{-3}qk/m_{\pi^+}^3$	$\text{Re}(M_{1+})$ $10^{-3}qk/m_{\pi^+}^3$	$\text{Re}(M_{1-})$ $10^{-3}qk/m_{\pi^+}^3$
$\gamma p \rightarrow \pi^0 p$ ($E_{\text{th}} = 144.7$ MeV)	B	-2.29	-0.15	5.94	-5.47
	$B + \text{FSI}$	-1.92	-0.18	6.45	-5.14
$\gamma p \rightarrow \pi^+ n$ ($E_{\text{th}} = 151.4$ MeV)	B	27.3	5.21	-9.74	5.71
	$B + \text{FSI}$	26.9	5.30	-10.1	5.48
$\gamma n \rightarrow \pi^- p$ ($E_{\text{th}} = 148.5$ MeV)	B	-31.2	-5.36	11.4	-7.66
	$B + \text{FSI}$	-29.7	-5.43	11.7	-7.44

TABLE II. Contributions of mechanisms, shown in Fig. 1, to the real part of the E_{0+} amplitude for $\gamma p \rightarrow \pi^0 p$ at threshold. The amplitudes are calculated in the Coulomb gauge and are given in units of $10^{-3}/m_{\pi^+}$. B denotes the contribution from the Born term alone, and (FSI) is the final-state interaction term defined in Eq. (2.2) and illustrated in Fig. 2.

$\gamma p \rightarrow \pi^0 p$ ($E_{\text{th}} = 144.7$ MeV)	Diagrams of Fig. 1						Sum
	(a)	(b)	(c)	(d)	(e)	(f)	
B	-1.26	-1.25	0.0	0.0	0.0	+0.22	-2.29
(FSI) $_{\pi^0 p}$	-0.10	+0.57	0.0	0.0	0.0	+0.05	+0.52
(FSI) $_{\pi^+ n}$	-0.53	-0.24	-3.07	+3.57	0.0	+0.10	-0.15
$B + \text{FSI}$	-1.89	-0.92	-3.07	+3.57	0.0	+0.37	-1.92

Here we have defined $\theta(x) = 1$ for $x \geq 0$ and $= 0$ otherwise. Recall the well-known relationship between the phase shift and the on-shell t matrix

$$\rho_{\pi N}(k_0) t_{\pi N \leftarrow \pi N}(k_0, k_0, E) = -e^{i\delta_{\pi N}} \sin \delta_{\pi N}, \quad (2.6)$$

Eqs. (2.5) lead to the half-off-shell relation

$$t_{\pi^0 p \leftarrow \pi n}(k_0, k, E) = e^{i\delta_{\pi^0 p}} \cos \delta_{\pi^0 p} \hat{K}_{\pi^0 p \leftarrow \pi N}(k_0, k, E). \quad (2.7)$$

We now return to consider the FSI integration, Eq. (2.2). Splitting the propagator into principal-value and δ -function parts, we have for $E > m_p + m_{\pi^0}$

$$(\text{FSI})_{\pi^0 p} = -i \rho_{\pi^0 p}(k_0) t_{\pi^0 p \leftarrow \pi^0 p}(k_0, k_0, E) B_{\pi^0 p \leftarrow \gamma p}(k_0, q) + \text{P} \int_0^\infty dk k^2 \frac{t_{\pi^0 p \leftarrow \pi^0 p}(k_0, k, E) B_{\pi^0 p \leftarrow \gamma p}(k, q)}{E - E_p(k) - E_{\pi^0}(k)} \quad (2.8a)$$

and

$$\begin{aligned} (\text{FSI})_{\pi^+ n} = & -i \theta(E - m_n - m_{\pi^+}) \rho_{\pi^+ n}(k_t) t_{\pi^0 p \leftarrow \pi^+ n}(k_0, k_t, E) B_{\pi^+ n \leftarrow \gamma p}(k_t, q) \\ & + \text{P} \int_0^\infty dk k^2 \frac{t_{\pi^0 p \leftarrow \pi^+ n}(k_0, k, E) B_{\pi^+ n \leftarrow \gamma p}(k, q)}{E - E_n(k) - E_{\pi^+}(k)}. \end{aligned} \quad (2.8b)$$

The θ function indicates that the wave function in the asymptotic region will not have the $\pi^+ n$ component if the energy is below its production threshold. Equation (2.8b) is the mathematical statement of this cusp effect. Substituting Eqs. (2.8) into Eq. (2.1) and using Eqs. (2.5) and (2.7), we have

$$\begin{aligned} M_{\pi^0 p \leftarrow \gamma p}(k_0, q) = & e^{i\delta_{\pi^0 p}} \cos \delta_{\pi^0 p} \left[B_{\pi^0 p \leftarrow \gamma p}(k_0, q) - i \theta(E - m_n - m_{\pi^+}) F_{\pi^0 p \leftarrow \pi^+ n}(k_0, k_t, E) B_{\pi^+ n \leftarrow \gamma p}(k_t, q) \right. \\ & \left. + \sum_{\pi N = \pi^0 p, \pi^+ n} \text{P} \int_0^\infty dk k^2 \frac{\hat{K}_{\pi^0 p \leftarrow \pi N}(k_0, k, E) B_{\pi N \leftarrow \gamma p}(k, q)}{E - E_N(k) - E_\pi(k)} \right]. \end{aligned} \quad (2.9)$$

TABLE III. Same as Table II, except for the charged pion production reactions.

Reaction (Threshold energy)		Diagrams of Fig. 1						Sum
		(a)	(b)	(c)	(d)	(e)	(f)	
$\gamma p \rightarrow \pi^+ n$ ($E_\gamma = 151.4$ MeV)	B	-1.75	-0.30	-0.04	+29.2	0.0	+0.16	+27.3
	FSI	-1.00	+0.36	-3.43	+3.40	0.0	+0.27	-0.40
	$B + \text{FSI}$	-2.75	+0.06	-3.47	+32.6	0.0	+0.43	+26.9
$\gamma n \rightarrow \pi^- p$ ($E_\gamma = 148.5$ MeV)	B	-0.29	-1.77	+0.06	-29.3	0.0	+0.15	-31.2
	FSI	-0.15	+1.29	+3.48	-3.30	0.0	+0.13	+1.45
	$B + \text{FSI}$	-0.44	-0.48	+3.54	-32.6	0.0	+0.28	-29.7

TABLE IV. Parameters of the form factors for the S_{11} and S_{31} πN separable potential: $v_{\pi N, \pi N}(k', k) = h_1(k')\lambda_1 h_1(k) + h_2(k')\lambda_2 h_2(k)$, where $h_1(k) = a_1 k^{m_1} / (k^2 + b_1^2)^{n_1}$ and $h_2(k) = a_2 k^{m_2} / (k^2 + b_2^2)^{n_2}$ (see Ref. 6 for details). a_1 is in units of (fm) $^{-2n_1+m_1+l+1}$ and a_2 is in units of (fm) $^{-2n_2+m_2+l+1}$.

$L_{2l, 2j}$	l	m_1	n_1	a_1	b_1 (fm $^{-1}$)	m_2	n_2	a_2	b_2 (fm $^{-1}$)	λ_1 ($=\lambda_2$)
S_{11}	0	0	3	100.0	2.5982	2	2	4.9518	2.8770	-1
S_{31}	0	0	2	3.0853	1.8056	2	2	1.9253	1.2746	+1

Equation (2.9) is our main result. We now consider the low-energy limit of Eq. (2.9). Here the on-shell t and K matrices can be related to the s -wave scattering length. By using the relation

$$\cot \delta_{\pi N}(k) \rightarrow 1/(a_{\pi N} k) \quad (2.10a)$$

and

$$\begin{aligned} a_{\pi^0 p} &= \frac{1}{3}(a^{T=1/2} + 2a^{T=3/2}) \\ &= \frac{1}{3}[0.245 + 2(-0.143)] = -0.01 \text{ fm} \end{aligned} \quad (2.10b)$$

the phase factor in Eq. (2.9) can be written near threshold as

$$e^{i\delta_{\pi^0 p}} \cos \delta_{\pi^0 p} \rightarrow \frac{1}{1 - ik_0(-0.01)} \rightarrow 1. \quad (2.10c)$$

We now note that the main feature of Eqs. (2.5b), (2.5c), and (2.9) is that the imaginary part is controlled by a θ function. In the energy region below the $\pi^+ n$ threshold, the second term of Eq. (2.9) vanishes and $\hat{K}_{\pi^0 p \leftarrow \pi N}$ [Eq. (2.5b)] reduces to the real function $K_{\pi^0 p \leftarrow \pi N}$. With Eq. (2.10c), we then expect that the multipole amplitude of Eq. (2.9) will be a purely real number below the $\pi^+ n$ production threshold. As the energy moves from below to above the $\pi^+ n$ threshold (151.4-MeV incident photon laboratory energy), we will see a sudden change in the imaginary part of the amplitude, and the cross section will show a rapid change. This is the dynamical formulation of the cusp effect. The visibility of this cusp effect of course depends on the underlying dynamics. This will be revealed explicitly in the next section.

Before we leave this section, let us just point out that if we drop the principal-value integral term and ignore the restriction due to the presence of the θ function in Eqs. (2.9) and (2.5b), we then have a formula identical to that of Davidson and Mukhopadhyay.¹⁰ If we further neglect the difference between \hat{K} and K matrices, defined in Eq. (2.5b), and extend the usual relationship between the K matrix and the scattering length to assume that $\rho_{\pi^+ n}(k_t) K_{\pi^0 p \leftarrow \pi^+ n}(k_0, k_t, E) \rightarrow -a_{\pi^0 p \leftarrow \pi^+ n} k_t$, we then get the commonly employed Eq. (1.1). Clearly the FSI due to the charge-exchange reaction generated from either one of these approaches is very different from what we have derived here. In particular, the usual analysis based on Eq. (1.1) is not, in general, compatible with a formulation retaining the full dynamics. For our explicit dynamical model, we will show that the deviation from Eq. (1.1) is large. We also expect the same conclusion from any other dynamical formulation.

We now turn to presenting our numerical results based on Eq. (2.9).

III. RESULTS AND DISCUSSIONS

With the given choice of the πN Hamiltonian,⁶ the only free parameters of our model are (1) the cutoff Λ of a monopole form factor $\Lambda^2/(\Lambda^2 + k^2)$ which regularizes the Born term, (2) the excitation strengths G_M and G_E for the $\Delta \leftrightarrow \gamma N$ transition. In Ref. 6, these parameters are determined from fitting the multipole amplitudes $M_{1+}(\frac{3}{2})$ and $E_{1+}(\frac{3}{2})$ that are dominated by the Δ excitation. The resulting model is able to give an overall good description of the cross section data for the $\gamma p \rightarrow \pi^0 p$, $\gamma p \rightarrow \pi^+ n$, and $\gamma n \rightarrow \pi^- p$ reactions up to about 400-MeV incident photon energy. An example of our results is shown in Fig. 4. It is seen that the total cross section data of $\gamma p \rightarrow \pi^0 p$ can be described very well with the following parameters: $\Lambda = 650$ MeV/ c , $G_M = 2.28$, and $G_E = 0.07$. The first question of interest in the present paper is whether the predictions of our model in the threshold-energy region are in agreement with the cross section data. In Fig. 5 we show that the prediction of the model, the solid curve, is in good agreement with the data. In the same figure the dashed curve is the prediction from the Born term alone in the absence of FSI. By comparing the solid and the dashed curves, it is clear that within our model the FSI indeed improves the agreement with the data, in particular in the region near the $\pi^+ n$ production threshold. The cusp effect, due to the opening of the $\pi^+ n$ channel, is needed for getting the right curvature of the cross section. Although this improvement is modest at the cross section level, it is particularly significant for the underlying multipole amplitudes. As might be expected, the cusp effect is most visible in the s -wave amplitude. This is explicitly shown in Fig. 5 for the cross section and Fig. 6 for the amplitude. The dash-dotted curve in Fig. 5 is the cross section calculated from the amplitude E_{0+} alone. The large difference between the solid and the

TABLE V. Individual contributions of S_{11} and S_{31} πN FSI to the E_{0+} multipole at threshold.

$\gamma p \rightarrow \pi^0 p$ ($E_\gamma = 144.7$ MeV)	$\text{Re}(E_{0+})$ $10^{-3}/m_{\pi^+}$
B	-2.29
$B + (\text{FSI})_{S_{11}}$	-2.62
$B + (\text{FSI})_{S_{31}}$	-1.60

dash-dotted curves indicates that an accurate treatment of the p -wave multipole amplitudes is also essential in order to obtain a correct understanding of the data. In Fig. 6 we demonstrate the cusp effect emerging from our calculation of the E_{0+} amplitude. The dashed curves are calculated from the Born term alone. When the full FSI effect of Eq. (2.9) is included, the calculated amplitude (solid curves) exhibits pronounced structures in the energy region near the π^+n threshold. As discussed in Sec. II and illustrated in Fig. 3, this is due to the shift of the pole position of the π^+n propagator from the real axis to the imaginary axis. The rapid increase in the imaginary part is due to the presence of the θ function in Eqs. (2.9) and (2.5). It is important to emphasize that the cusp effect exhibited here is generated by keeping the complete πN dynamics, and is radically different from that based on Eq. (1.1).

In Fig. 7, we show the FSI effect in determining M_{1+} and M_{1-} amplitudes in the low-energy region. Apparently, the FSI is not completely negligible. But we find that with the FSI included, it is still a good approximation to assume that M_{1+}/qk and M_{1-}/qk are constants, as assumed in the analyses of Refs. 1 and 2. The importance of the FSI is more clearly seen in the results for the differential cross section shown in Fig. 8. Here we also see that our model is consistent with the published experimental data.¹ Obviously more precise measurements are needed for an accurate determination of the multipole amplitudes.

To see the dynamical content of our calculation, we now focus on the results at threshold. In Table I, we show the FSI effects in determining the multipole amplitudes for $\gamma p \rightarrow \pi^0 p$, $\gamma p \rightarrow \pi^+ n$, and $\gamma n \rightarrow \pi^- p$. The FSI effect in charged pion production is small, and hence our full calculations do not deviate significantly from the predictions of the low-energy theorem. The FSI effect on the E_{0+} multipole for neutral pion production (first row) is $+0.37$. It is of opposite sign to the (FSI) term of Eq. (1.1) employed in the analyses of Refs. 1 and 2. Our value $E_{0+} = -1.92$ is close to the measured value -1.5 of Eq. (1.2). We therefore have demonstrated that with a dynamical treatment of the final-state interaction, it is possible to describe the π^0 photoproduction data without introducing any modification of the low-energy theorem in describing the basic pion photoproduction mechanism (as suggested in Ref. 14).

To further understand our result, it is necessary to examine the role of each mechanism, shown in Fig. 1, in determining the FSI effect. This is presented in Table II. We note that there are large cancellations between different mechanisms. In particular, both mechanisms (c) and (d) have large contributions to the FSI term involving the π^+n intermediate state, but they have opposite signs and almost cancel each other. This explains why we have a very surprising result that the FSI involving the $\pi^0 p$ intermediate state is *larger* than that due to the π^+n intermediate state. This is seen in comparing the numbers in the last column of Table II. If the prescription of Eq. (1.1) is used, the contribution from each mechanism will be scaled by the same factor " $k, a_{\pi^+n \rightarrow \pi^0 p}$." This, taken together with the fact that the charged pion

photoproduction Born term is dominated by the contact interaction (see Table III), leads one to expect the opposite behavior from ours—as commonly assumed in experimental analyses. The results shown in Table II clearly indicate the fundamental difference between a calculation retaining the full dynamics, and the approach based on Eq. (1.1). In Table III we also show that the cancellation between mechanisms (c) and (d) also occurs for charged pion production. We should emphasize here that this somewhat unexpected result could depend on the three-dimensional reduction introduced in Ref. 6 to deduce from the Feynman amplitudes unitary and gauge invariant current matrix elements which are consistent with the considered πN scattering theory. It is well known that the three-dimensional reduction of a field theory is not unique. Hence, further investigations are needed to determine whether this cancellation is specific to our approach or is a general property of the basic dynamics.

At threshold, the FSI is only due to the πN interaction in the S_{11} and S_{31} channels. The parameters used in our calculation are displayed in Table IV. In Table V we show that the FSI due to the S_{31} is as important as that due to the S_{11} channel. Again there is a large cancellation between these two different FSI effects.

We now note that the FSI effect listed in the last column of Table II is very close to one of the results obtained by Yang⁷ (the BL result in his Table I). Perhaps this is due to the fact that both models approach the same static limit which dominates the mechanisms in the threshold-energy region. Our main new contribution is to reveal in more detail the dynamical origins of the FSI effect, and show that Eq. (1.1) commonly used in the analysis of the data is not compatible with a dynamical model. In addition, we have explicitly demonstrated, analytically in Sec. II and numerically in Figs. 5 and 6, how the cusp effect arises from the mass difference between the intermediate $\pi^0 p$ and $\pi^+ n$ states.

To close, we need to emphasize that the FSI calculation is sensitive to the off-energy-shell behavior of the employed πN model. This has been pointed out by Yang.⁷ The phenomenological separable πN model employed in our study is certainly not very satisfactory theoretically, although it can accurately describe the πN phase shifts up to 500 MeV. In the future, it is necessary to investigate the problem using a πN model constructed also from an effective Lagrangian which accommodates the low-energy theorems. Only by using such a full consistent description of both the hadronic and electromagnetic matrix elements, can the low-energy theorem be truly tested.

ACKNOWLEDGMENTS

We would like to thank A. Fujii and I. Towner for useful discussions. T.-S.H.L. would like to thank E. Vogt and the TRIUMF theory group for their warm hospitality and financial support. This work was supported in part by the Natural Sciences and Engineering Research Council of Canada, and by the U.S. Department of Energy, Nuclear Physics Division, under Contract W-31-109-ENG-38.

*Permanent address: Argonne National Laboratory, Argonne, IL 60439.

¹E. Mazzucato *et al.* Phys. Rev. Lett. **57**, 3144 (1986).

²P. Argan *et al.* Phys. Lett. B **206**, 4 (1988); Nico de Bottom (private communication).

³S. L. Adler and R. F. Dashen, *Current Algebras and Applications to Particle Physics* (Benjamin, New York, 1968).

⁴H. Tanabe and K. Ohta, Phys. Rev. C **31**, 1876 (1985).

⁵S. N. Yang, J. Phys. G **11**, L205 (1985).

⁶S. Nozawa, B. Blankleider, and T.-S. H. Lee (unpublished).

⁷S. N. Yang, Phys. Rev. C (to be published).

⁸R. H. Dalitz and S. F. Tuan, Ann. Phys. (NY) **10**, 307 (1960).

⁹G. Höhler, *Pion-Nucleon Scattering: Methods and Results of*

Phenomenological Analyses, Vol. 9b2 of *Landolt-Börnstein Series on Numerical Data and Functional Relationships in Science and Technology*, edited by H. Schopper (Springer-Verlag, Berlin, 1983).

¹⁰R. Davidson and N. C. Mukhopadhyay, Phys. Rev. Lett. **60**, 748 (1988).

¹¹M. Araki, Phys. Lett. B **219**, 135 (1989).

¹²K. M. Watson, Phys. Rev. **95**, 228 (1954).

¹³M. L. Goldberger and K. M. Watson, *Collision Theory* (Wiley, New York, 1964).

¹⁴L. M. Nath and S. K. Singh, Phys. Rev. C **39**, 1207 (1989).

¹⁵D. Menze, W. Pfeil, and R. Wilcke, *ZAED Compilation of Pion Photoproduction Data*, University of Bonn, 1977.